The Effect of a CGO Barrier Layer on the Performance of LSM/YSZ SOFC Cathodes

Kammer Hansen, Kent; Menon, Mohan; Knudsen, Jesper; Bonanos, Nikolaos; Mogensen, Mogens Bjerg

Published in:
Electrochemical Society. Journal

Link to article, DOI:
10.1149/1.3273194

Publication date:
2010

Document Version
Publisher's PDF, also known as Version of record

Journal of The Electrochemical Society, **157** (3) B309-B313 (2010)
0013-4651/2009/157(3)/B309/5/$28.00 © The Electrochemical Society

The Effect of a CGO Barrier Layer on the Performance of LSM/YSZ SOFC Cathodes

K. Kammer Hansen,*,z M. Menon,* J. Knudsen, N. Bonanos, and M. Mogensen*

Fuel Cells and Solid State Chemistry Division, Risø National Laboratory for Sustainable Energy, Technical University of Denmark, DK-4000 Roskilde, Denmark

Strontium-substituted lanthanum manganite/yttria-stabilized zirconia (LSM/YSZ) solid oxide fuel cell (SOFC) composite electrodes were fabricated with slurry spraying on both sides on either pure YSZ electrolyte foils or YSZ electrolyte foils with a cerium–gadolinium oxide (CGO) barrier layer made by spin coating. Electrochemical impedance spectroscopy was used to evaluate the performance of the LSM/YSZ composite electrodes. It was shown that the CGO barrier layer affects both the performance of the LSM/YSZ composite electrodes and the series resistance of the cells. This indicates that the cathode–electrolyte interface and the barrier layer–electrolyte interface have a large influence on the performance of LSM/YSZ composite electrodes.
 [DOI: 10.1149/1.3273194]

Manuscript submitted August 17, 2009; revised manuscript received November 13, 2009. Published December 31, 2009.

The solid oxide fuel cell (SOFC) is a device that converts the chemical energy directly into heat and electricity. The SOFC is traditionally constructed from a strontium-substituted lanthanum manganite/yttria-stabilized zirconia (LSM/YSZ) composite cathode, a YSZ electrolyte, and a Ni/YSZ composite anode. To lower the operation temperature of the SOFC, new electrode materials are needed, especially on the cathode side. The cathodes that perform better than the traditional LSM/YSZ cathodes are Fe–Co-based perovskites.[1] However, these types of cathodes react with the zirconia-based electrolyte.[2] To use Fe–Co-based perovskite cathodes, a barrier layer between the cathode and the electrolyte is therefore needed to prevent a reaction. Several attempts to use a cerium–gadolinium oxide (CGO)-based barrier layer have been done.[3-7] It has been shown that a CGO barrier layer prevents the formation of a reaction layer between a Fe–Co-based cathode and a zirconia-based electrolyte.

In this study, the effect of a spin-coated CGO barrier layer between the YSZ electrolyte and an LSM/YSZ cathode was studied using electrochemical impedance spectroscopy (EIS) to investigate the effect of the CGO barrier layer as such. This was possible compared to LSM/YSZ electrodes put directly onto YSZ as strontium-substituted lanthanum manganite (LSM) does not react with YSZ. It is not possible to study the effect of the CGO barrier as such using cobalt-based perovskites as they react with YSZ and, therefore, cannot be put directly onto YSZ.

Experimental

The LSM25 $[(La_{0.75}Sr_{0.25})_{0.95}MnO_{3+\delta}]$ powder was used as received from Haldor Topsøe A/S. The LSM25 powder was synthesized using drip pyrolysis. The phase purity of the LSM25 powder was confirmed by powder X-ray diffraction. For the synthesis of the LSM25 powder, the following metal nitrates were used: $La(NO_3)_3 \cdot 6H_2O$ (Alfa Aesar, 99.9%), $Sr(NO_3)_2$ (Alfa Aesar, 99%), and $Mn(NO_3)_2 \cdot 4H_2O$ (Alfa Aesar, 98%). Aqueous solutions of the metal nitrates were made, and the concentrations of these solutions were determined using gravimetry. The YSZ electrolyte powder was also used as received from the supplier (Tosoh). Cathode slurries were prepared by mixing LSM25 and YSZ, in a 50 wt % ratio, with a dispersant and a binder and by ballmilling for 24 h. The dispersant was polyvinylpyrrolidone (PVP, Sigma Aldrich). The binder was a mixture of Mowital B60H, PVP, dibutylphthalat (Merck), and poly(ethylene glycol) (Merck). A 3% (w/w) dispersant and a 2% (w/w) binder were added to the slurries. The mean particle size of the slurry was 0.9 μm. Precursor solutions for CGO were prepared by dissolving $Ce(NO_3)_3$ (Alfa Aesar, 99.5%), $Gd(NO_3)_3$ (Alfa Aesar, 99.9%), nitric acid, and ethylene glycol in water and by heating the mixture at 80°C. The heating was stopped when the room temperature viscosity of the solution reached 50 mPa s. The room temperature viscosity was determined using a Haake Rheostress 600 rheometer. Spin coating by the CGO precursor solution was performed using a WS-400A-8NPP/lite spin coater from Laurell Technologies. After spin coating, the samples were heat-treated at 550°C for 2 h. To ensure the complete coverage of the tape surfaces, spin coating and heat-treatment were repeated four times. Both surfaces of the tapes were coated. The resulting film had a thickness of 150 nm. Details of the CGO thin-film fabrication can be found in a previous publication.[8] Symmetric cells comprised of porous LSM/YSZ/dense YSZ/porous LSM/YSZ were prepared by spraying, with a spraying robot, on both sides of dense-sintered electrolyte tapes. The following were used as electrolyte tapes: (*i*) YSZ tapes and (*ii*) CGO thin-film-coated YSZ tapes. The symmetrical cells with and without a CGO barrier layer were sprayed in one go to make the fabrication of the symmetrical cells as uniform as possible. The symmetrical cells were sintered at 1050°C/2 h. At this sintering temperature, CGO does not react with YSZ.[9] The YSZ tapes were fabricated using a tape casting followed by sintering at 1450°C/8 h. Tosoh YSZ powder was used for the fabrication of the YSZ tapes. Micrographs of the symmetrical cells were recorded on a Zeiss 1540XB field-emission gun-scanning electron microscope equipped with a Gemini column in-lens detector and an energy dispersive spectroscopy (EDS) spectrometer for an element analysis. The EIS was performed using a Solartron 1260 impedance analyzer. The samples were mounted in a setup with platinum meshes kept in contact with the cells with a spring load. Before mounting the samples, Pt-paste (Engelhard) was added on top of the cells and sintered in situ at 800°C. The setup used for the measurements has been described elsewhere.[10] The EIS was recorded on the samples as follows. The frequency window spanned was 1 MHz to 0.05 or 0.01 Hz depending on the temperature. The lowest frequencies were only recorded at the lowest measured temperatures. Five points were measured at each decade. An amplitude of 24 mV was used throughout. The measurements were done at temperatures of 800, 700, and 600°C in the above order. The measurements were done in either 100% O_2, 10% O_2 in He, or 1% O_2 in He. All measurements were done on four symmetrical cells. The fitting of the data was done using the PC-DOS program "equivcrt" by Boukamp.[11] The fittings were done with the circuit $R_s(R_1Q_1)(R_2Q_2)(R_3Q_3)$, where R is a resistance and Q is a constant phase element with the admittance

$$Y = Y_0(j\omega/\omega_0)^n \quad [1]$$

* Electrochemical Society Active Member.
z E-mail: kkha@risoe.dtu.dk

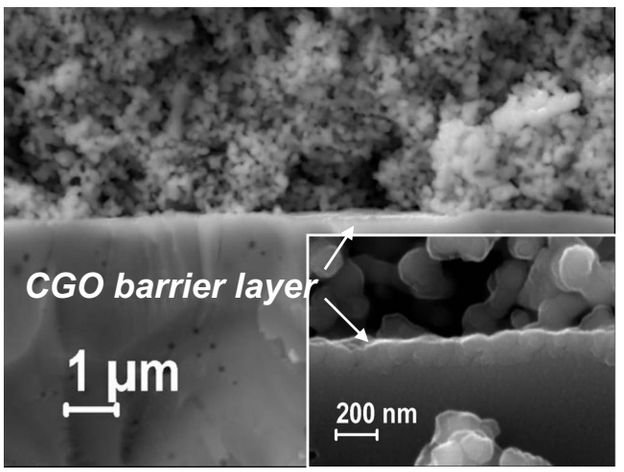

Figure 1. SEM micrographs of a symmetrical cell with a CGO barrier layer. The inset is a high resolution micrograph of the barrier layer.

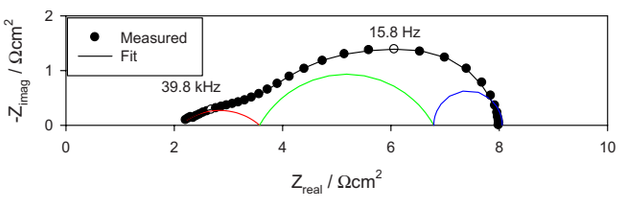

Figure 2. (Color online) EIS spectrum of a symmetrical cell (porous LSM/YSZ/dense YSZ/porous LSM/YSZ) in 100% O_2 at 600°C, i.e., the response is from two electrodes in series with the electrolyte resistance. The colored lines are deconvolution of the data; the solid black line is the full fit.

the results of the fitting, the near-equivalent capacitance C_ω and the summit frequency F_{max} were calculated using the equations[14]

$$C_\omega = R^{(1-n)/n} Y_0^{1/n} \quad [2]$$

$$F_{max} = \frac{1}{2\pi}(RY_0)^{1/n} \quad [3]$$

Results

Figure 1 shows a micrograph of the LSM/YSZ electrode on a YSZ tape with a CGO barrier layer. The presence of the Ce/Gd-containing thin film was confirmed by the EDS point analysis. The CGO barrier layer is seen to be homogenous with an estimated thickness of approximately 150 nm. This is most clearly seen in the inset. Figure 2 gives an example of an impedance spectrum of a symmetrical cell, together with the results of the fitting. The data presented in Fig. 2 were recorded on a symmetrical cell without a CGO barrier layer in 100% oxygen at 600°C. It is seen that the spectrum consists of three arcs. In general, the results from the EIS measurements could be fitted with an equivalent circuit with three (R_Q) elements in series, together with a series resistance R_s. The results of the fitting, in terms of R values of the individual arcs, are given in Tables I-VI together with F_{max} and C_ω. The variation in the data is based on measurements and fittings on four symmetrical cells. It is seen that all the arcs are P_{O_2} dependent. The P_{O_2} dependence is largest for the medium and low frequency arcs (see also Fig. 3). The magnitude of the individual arcs is larger for the cells with the CGO barrier layer than for the cells without the CGO barrier layer; this is illustrated in Fig. 4. The medium frequency arc is observed to be the arc that depends the less on the presence or absence of a CGO barrier layer. In contrast to this, the high and low frequency arcs are seen to depend strongly on the presence or absence of a CGO barrier layer. The n values are 0.45 for the high frequency arc, 0.67 for the medium frequency arc, and 1 for the low frequency arc. The temperature dependence is illustrated in Fig. 5. The area specific resistance (ASR) is seen to increase with decreasing temperature.

The near-equivalent capacities for all three arcs are smallest for the cells with a CGO barrier layer. The summit frequencies of the three arcs all depend on the presence or absence of a CGO barrier layer. The summit frequencies for the high frequency arc are largest

Table I. The R, C_ω, and F_{max} values of the individual arcs for symmetrical cells without a CGO barrier layer in 100% oxygen. R is given in Ω cm², C_ω is in mF cm^{-2} unless otherwise stated, and F_{max} is in Hz.

	High frequency			Medium frequency			Low frequency		
100% temperature (°C)	R_1	C_ω (μm)	F_{max}	R_2	C_ω	F_{max}	R_3	C_ω	F_{max}
600	1.50 ± 0.01	2.8	9699	3.30 ± 0.07	0.30	39	1.28 ± 0.03	3.7	8.4
700	0.43 ± 0.006	9.0	10,577	0.47 ± 0.08	0.34	233	0.23 ± 0.08	2.1	80
800	0.12 ± 0.003	2.3	138,000	0.11 ± 0.004	0.12	2912	0.07 ± 0.006	0.93	55

Table II. The R, C_ω, and F_{max} values of the individual arcs for symmetrical cells without a CGO barrier layer in 10% oxygen in helium. R is given in Ω cm², C_ω is in mF cm^{-2} unless otherwise stated, and F_{max} is in Hz.

	High frequency			Medium frequency			Low frequency		
10% temperature (°C)	R_1	C_ω (μm)	F_{max}	R_2	C_ω	F_{max}	R_3	C_ω	F_{max}
600	1.66 ± 0.006	4.9	4940	5.62 ± 0.08	0.57	12.7	1.84 ± 0.02	8.1	2.7
700	0.40 ± 0.04	15.2	7439	0.93 ± 0.05	0.44	102	0.37 ± 0.03	3.8	26
800	0.14 ± 0.002	8.2	35,707	0.19 ± 0.01	0.29	745	0.10 ± 0.002	2.0	197

where Y_0 and n are found from the fitting. ω is the cyclic frequency.[a] In the fitting, the n values were at first allowed to vary freely. After fitting, all the data and the averages of the n values were found. The data were then fitted again using the averages of the n values. From

[a] The results from EIS measurements on composite electrodes are known to be complex and consist of several more or less overlapping arcs (see 10). In our case, fitting with three R_Q's in a series with a resistance gave the best results, although we are aware that other models have been suggested.[12,13]

Table III. The R, C_ω, and F_{max} values of the individual arcs for symmetrical cells without a CGO barrier layer in 1% oxygen in helium. R is given in Ω cm^2, C_ω is in mF cm^{-2} unless otherwise stated, and F_{max} is in Hz.

	High frequency			Medium frequency			Low frequency		
1% temperature (°C)	R_1	C_ω (μm)	F_{max}	R_2	C_ω	F_{max}	R_3	C_ω	F_{max}
600	2.06 ± 0.004	7.7	2418	10.7 ± 0.14	1.00	3.76	4.82 ± 0.04	12.6	0.67
700	0.55 ± 0.002	11.9	6057	1.95 ± 0.01	0.83	24.9	0.70 ± 0.006	10.0	5.6
800	0.18 ± 0.01	7.7	30,800	0.41 ± 0.01	0.55	180	0.15 ± 0.01	2.0	42.8

Table IV. The R, C_ω, and F_{max} values of the individual arcs for symmetrical cells with a CGO barrier layer in 100% oxygen. R is given in Ω cm^2, C_ω is in mF cm^{-2} unless otherwise stated, and F_{max} is in Hz.

	High frequency			Medium frequency			Low frequency		
100% temperature (°C)	R_1	C_ω (μm)	F_{max}	R_2	C_ω	F_{max}	R_3	C_ω	F_{max}
600	2.72 ± 0.08	1.0	14,032	4.11 ± 0.10	0.23	40.1	1.90 ± 0.07	2.2	4.21
700	0.64 ± 0.04	2.1	28,041	0.64 ± 0.03	0.19	313	0.36 ± 0.03	1.3	81.2
800	0.18 ± 0.008	1.1	208,000	0.13 ± 0.008	0.09	3412	0.09 ± 0.006	0.66	616

for the cells with a CGO barrier layer. The summit frequencies for the medium frequency arc are almost unaffected by the presence or absence of a CGO barrier layer. The summit frequencies for the low frequency arc are largest for the cells without a CGO barrier layer, even though the effect is rather small.

The Arrhenius plots for the total ASR without or with a CGO barrier layer are given in Fig. 6 and 7. The total ASR increases with decreasing P_{O_2}.

The activation energies for the individual arcs are given in Table VII. The activation energies depend on both the P_{O_2} and the presence or absence of a CGO barrier layer. The activation energies are largest for the cells with a CGO barrier layer. The activation energies are seen to increase with increasing P_{O_2}.

The series resistance also depends on the presence or absence of a CGO barrier layer. In a pure YSZ electrolyte, the series resistance is around 1.8 Ω cm^2 at 600°C, whereas it is around 5.7 Ω cm^2 at 600°C when a CGO barrier layer is present.

Discussion

The performance of the electrodes, as reflected by the ASR values, is on the level with the best slurry-sprayed LSM/YSZ composite cathodes for the cells without a CGO barrier layer.[15-19] The cells with a CGO barrier layer have a much lower activity. The high frequency arc in the impedance plot is, according to literature, due to the transfer of oxygen intermediates/oxide ions between the LSM cathode and the YSZ electrolyte and through the YSZ of the composite.[10,20,21] This agrees well with the calculated equivalent capacitances, which are in the range expected for a double-layer capacitance.[22] The activation energy for the high frequency arc is slightly higher for the cells with a CGO barrier layer than for the cells without a CGO barrier layer. The magnitude of this arc is much larger for the cells with a CGO barrier layer than for the cells without a CGO barrier layer at all conditions used in this study. This indicates that the CGO barrier layer slows down the electrode–electrolyte exchange reaction. The near-equivalent capacity is higher

Table V. The R, C_ω, and F_{max} values of the individual arcs for symmetrical cells with a CGO barrier layer in 10% oxygen in helium. R is given in Ω cm^2, C_ω is in mF cm^{-2} unless otherwise stated, and F_{max} is in Hz.

	High frequency			Medium frequency			Low frequency		
10% temperature (°C)	R_1	C_ω (μm)	F_{max}	R_2	C_ω	F_{max}	R_3	C_ω	F_{max}
600	2.90 ± 0.13	1.7	7597	7.38 ± 0.60	0.45	11	3.65 ± 0.10	5.5	2
700	0.70 ± 0.04	3.0	17,468	1.32 ± 0.09	0.38	76	0.55 ± 0.02	3.9	18
800	0.21 ± 0.03	1.9	90,619	0.28 ± 0.02	0.20	674	0.14 ± 0.02	1.8	145

Table VI. The R, C_ω, and F_{max} values of the individual arcs for symmetrical cells with a CGO barrier layer in 1% oxygen in helium. R is given in Ω cm^2, C_ω is in mF cm^{-2} unless otherwise stated, and F_{max} is in Hz.

	High frequency			Medium frequency			Low frequency		
1% temperature (°C)	R_1	C_ω (μm)	F_{max}	R_2	C_ω	F_{max}	R_3	C_ω	F_{max}
600	3.29 ± 0.19	2.8	4102	11.9 ± 0.84	0.75	4.2	8.23 ± 0.33	8.7	0.53
700	0.81 ± 0.07	4.6	9870	2.30 ± 0.17	0.65	24	1.16 ± 0.05	8.2	4.1
800	0.25 ± 0.03	4.1	34,403	0.51 ± 0.04	0.43	172	0.22 ± 0.02	6.2	32

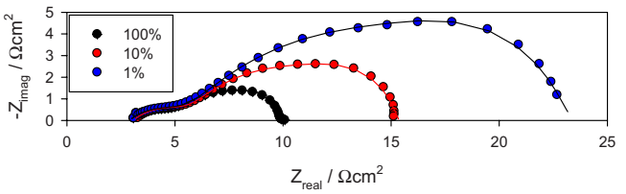

Figure 3. (Color online) EIS spectra of a symmetrical cell with a CGO barrier layer recorded at 600°C in 100% O_2, 10% O_2 in He, and 1% O_2 in He. The solid lines are fitted data; dots are measured data.

for the cells without a CGO barrier layer than with a ceria barrier layer. This indicates that there are more contact points between the LSM/YSZ cathode and the electrolyte when put directly onto YSZ than when put on a YSZ electrolyte with a CGO barrier layer. The P_{O_2} dependence of the high frequency arc is very weak, approximately 1/16. This is another indication that the high frequency arc involves oxide anions and not oxygen, as it is almost P_{O_2} independent. The activation energy of the medium frequency arc is also dependent on the type of the cell, indicating that this process is affected by the CGO barrier layer. This arc could be a diffusion of oxide anions through the bulk or the surface of the electrode.[10,20,21] If surface diffusion is the case, the medium frequency arc could depend on the presence of a CGO barrier layer if the process occurs close to the electrode–electrolyte interface. The P_{O_2} dependence of this arc is around 1/4. The low frequency arc is also dependent on the presence or absence of a CGO barrier layer. The magnitude of the low frequency arc is larger when the CGO layer is present than when it is absent. This arc could be due to a slow redox reaction at the surface of the electrode.[10,20,21] If this process occurs close to the triple-phase boundary, it should depend on the presence or absence of a CGO barrier layer. The P_{O_2} dependence of this arc is around 1/4, as predicted for a charge-transfer reaction of the type[23]

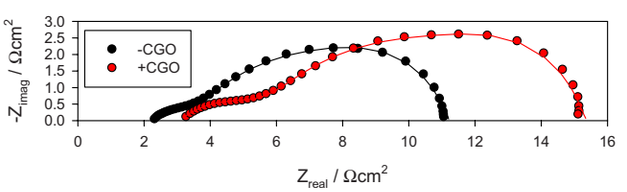

Figure 4. (Color online) EIS spectra of symmetrical cells with or without a CGO barrier layer recorded at 600°C in 10% O_2 in He. The solid lines are fitted data; dots are measured data.

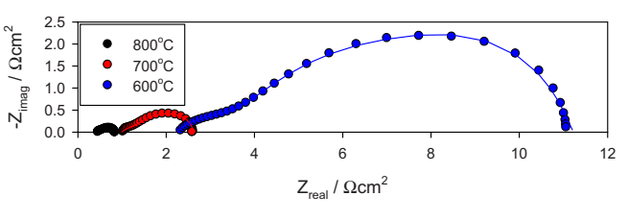

Figure 5. (Color online) EIS spectra of a symmetrical cell recorded at 600, 700, and 800°C in 10% O_2 in He. The solid lines are fitted data; dots are measured data.

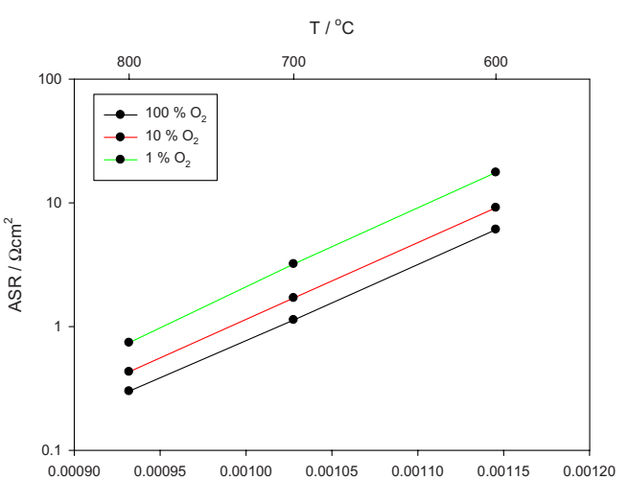

Figure 6. (Color online) Arrhenius plots of the total ASR as a function of temperature for the cells without a CGO barrier layer. The total ASR increases with decreasing P_{O_2}.

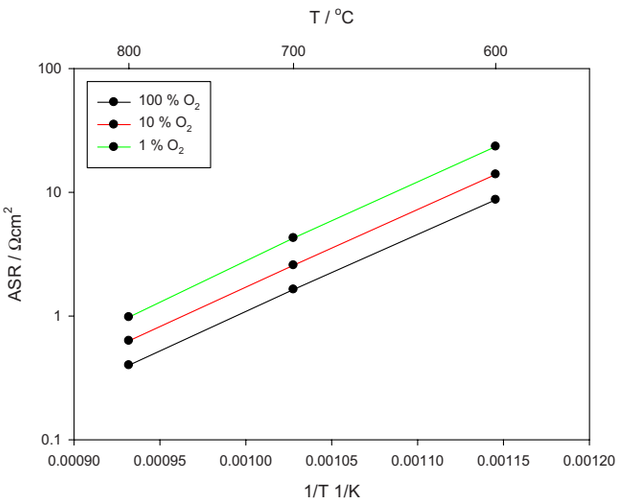

Figure 7. (Color online) Arrhenius plots of the total ASR as a function of temperature for the cells with a CGO barrier layer. The total ASR increases with decreasing P_{O_2}.

$$O_{ads} + 2e^- + V_O^{\cdot\cdot} \leftrightarrow O_O^x \quad [4]$$

The calculated near-equivalent capacitance of this arc is also in the range predicted for a chemical capacitance.[22] That all the arcs are dependent on the presence or absence of a CGO barrier layer indicates that most of the processes occur close to the electrode–electrolyte interface. An arc from the CGO barrier itself is not observed as all the arcs are P_{O_2} dependent.

That the cells with a CGO barrier layer perform worse than the cells without a CGO barrier layer shows that the reactivity of LSM with YSZ is low, as expected. The worse performance of the cells with CGO could be due to less contact points between the LSM/YSZ cathode and the CGO barrier layer compared to the amount of contact points between the LSM/YSZ cathodes and the YSZ elec-

Table VII. Activation energies of the two types of cells in different atmospheres. −CGO is without a CGO barrier layer and +CGO is with a CGO barrier layer.

	High (R_1) (eV)	Medium (R_2) (eV)	Low (R_3) (eV)
1% O_2 + CGO	1.04 ± 0.01	1.27 ± 0.04	1.46 ± 0.02
1% O_2 − CGO	0.98 ± 0.01	1.31 ± 0.01	1.40 ± 0.01
10% O_2 + CGO	1.06 ± 0.01	1.32 ± 0.04	1.32 ± 0.04
10% O_2 − CGO	1.00 ± 0.03	1.37 ± 0.03	1.18 ± 0.01
100% O_2 + CGO	1.09 ± 0.02	1.39 ± 0.02	1.23 ± 0.01
100% O_2 − CGO	1.02 ± 0.07	1.37 ± 0.03	1.18 ± 0.05

trolyte. An effect of the electrolyte pretreatment on the performance of SOFC electrodes has been found before.[24,25] This shows that the barrier layer in itself also has an effect on the activity of the electrodes, and not only prevents a reaction between the electrode and the electrolyte.

The series resistance is also marked higher for the cells with a CGO barrier layer than for the cells without a CGO barrier layer. The resistance of a 150 nm thick CGO layer can be calculated from the specific conductivity of the CGO electrolyte, $\sigma = 0.0167$ S/cm at 600°C [26] from the equation

$$R_e = L/\sigma \quad [5]$$

where L is the thickness of the barrier layer. At 600°C, this gives a contribution of 1 $m\Omega$ cm^2. This is much lower than the difference in the series resistance between the cells with and without the CGO barrier layer observed in this study. This shows that the increased series resistance is not due to the barrier layer in itself, but due either to the bad adhesion of the CGO barrier layer to the YSZ electrolyte or to the reaction between the CGO barrier layer and the YSZ electrolyte. If the increased series resistance is due to bad adhesion, the CGO barrier layer must be sintered at higher temperatures than used in this study to obtain a better contact between the CGO barrier layer and the YSZ electrolyte. However, too high sintering temperatures must be avoided as this leads to the formation of a reaction layer between ceria and zirconia.[27] Other ways to improve the contact between the CGO barrier layer and the YSZ electrolyte could be to change the precursor solution or to use other techniques than spin coating to apply the CGO barrier layer.[6]

Conclusion

The addition of a CGO barrier layer between the electrolyte and the cathode decreases the performance of the LSM/YSZ composite electrodes. This is probably due to an interface effect. The series resistance increases significantly when a CGO barrier layer is added between the YSZ electrolyte and the LSM/YSZ cathode. This could be due to the bad adhesion of the CGO barrier layer to the YSZ electrolyte.

Acknowledgments

Colleagues at the Fuel Cells and Solid State Chemistry Division were thanked for fruitful discussions. Financial support from the Energinet.dk through PSO-R&D-project no. 2006-1-6493 was gratefully acknowledged.

Risø National Laboratory for Sustainable Energy assisted in meeting the publication costs of this article.

References

1. J. M. Ralph, C. Rossignol, and R. Kumar, *J. Electrochem. Soc.*, **150**, A1518 (2003).
2. Y. Liu, W. Rauch, S. Zha, and M. Liu, *Solid State Ionics*, **166**, 261 (2004).
3. A. O. Stoermer, J. L. M. Rupp, and L. J. Gauckler, *Solid State Ionics*, **177**, 2075 (2006).
4. A. Mai, V. A. C. Haanappel, F. Tietz, and D. Stöver, *Solid State Ionics*, **177**, 2103 (2006).
5. J. C. Ruiz-Morales, J. Canales-Vázquez, B. Ballesteros-Pérez, J. Peña-Martínez, D. Marrero-López, J. T. S. Irvine, and P. Núñez, *J. Eur. Ceram. Soc.*, **27**, 4223 (2007).
6. N. Jordan, W. Assenmacher, S. Uhlenbruck, V. A. C. Haanappel, H. P. Buchkremer, D. Stöver, and W. Mader, *Solid State Ionics*, **179**, 919 (2008).
7. S. Bebelis, V. Kournoutis, A. Mai, and F. Tietz, *Solid State Ionics*, **179**, 1080 (2008).
8. L. Rose, M. Menon, K. Kammer, O. Kesler, and P. H. Larsen, *Adv. Mater. Res.*, **15–17**, 293 (2007).
9. Z. Duan, M. Yang, A. Yan, Z. Hou, Y. Dong, Y. Chong, M. Cheng, and W. Yang, *J. Power Sources*, **160**, 57 (2006).
10. M. J. Jørgensen and M. Mogensen, *J. Electrochem. Soc.*, **148**, A433 (2001).
11. B. A. Boukamp, *Solid State Ionics*, **20**, 31 (1986).
12. S. Bebelis, N. Kotsionopoulos, A. Mai, and F. Tietz, *Solid State Ionics*, **177**, 1843 (2006).
13. F. S. Baumann, J. Fleig, H.-U. Habenmeier, and J. Maier, *Solid State Ionics*, **177**, 1071 (2006).
14. T. Jacobsen, B. Zachau-Christiansen, L. Bay, and S. Skaarup, in *Proceedings of the 17th International Symposium on Materials Science; High Temperature Electrochemistry: Ceramics and Metals*, F. W. Poulsen, J. J. Bentzen, T. Jacobsen, E. Skov, and M. J. L. Østergård, Editors, Risø National Laboratory, Roskilde, Sweden, p. 29 (1996).
15. T. Kenjo and M. Nishiya, *Solid State Ionics*, **57**, 295 (1992).
16. M. J. L. Østergård, S. Primdahl, C. Bagger, and M. Mogensen, *Electrochim. Acta*, **40**, 1971 (1995).
17. M. J. Jørgensen, S. Primdahl, C. Bagger, and M. Mogensen, *Solid State Ionics*, **139**, 1 (2001).
18. S. Linderoth, in *Proceedings of the Fourth European SOFC Forum*, A. J. McEvoy, Editor, Lucerne, Switzerland, p. 19 (2000).
19. W. G. Wang, R. Barfod, P. H. Larsen, K. Kammer, J. J. Bentzen, P. V. Hendriksen, and M. Mogensen, *Proceedings of the Eighth International Symposium on Solid Oxide Fuel Cells (SOFC-VIII)*, S. C. Singhal and M. Dokiya, Editors, PV 2003-07, pp. 400–408, The Electrochemical Society, Pennington, NJ (2003).
20. E. Siebert, A. Hammouche, and M. Kleitz, *Electrochim. Acta*, **40**, 1741 (1995).
21. L. O. Jerdal, Ph.D. Thesis, Norwegian University of Science and Technology, Norway (1998).
22. S. B. Adler, J. A. Lane, and B. C. H. Steele, *J. Electrochem. Soc.*, **143**, 3554 (1996).
23. Y. Takeda, R. Kanno, M. Noda, T. Tomida, and O. Yamamoto, *J. Electrochem. Soc.*, **134**, 2656 (1987).
24. L. A. Dunyushkina and S. B. Adler, *J. Electrochem. Soc.*, **152**, A2040 (2005).
25. K. Kammer and M. Mogensen, Unpublished work.
26. C. Xia and M. Liu, *Solid State Ionics*, **144**, 249 (2001).
27. M. Mogensen, N. M. Sammes, and G. A. Tompsett, *Solid State Ionics*, **129**, 63 (2000).